Artificial Organs
24(2):137–147, Blackwell Science, Inc.

Biodesign of a Skeletal Muscle Flap as a Model for Cardiac Assistance

Victor V. Nikolaychik, Valeri S. Chekanov, Irene Hernandez, Matthew D. Silverman, and Peter I. Lelkes

University of Wisconsin Medical School and Milwaukee Heart Project, Milwaukee, Wisconsin, U.S.A.

Abstract: In using autologous muscles for cardiac assistance, it is crucial to reduce ischemia-reperfusion injury in the surgically traumatized skeletal muscle. In adult sheep, we developed a simple model of surgically designed 2 latissimus dorsi muscle leaflets by modifying the vascular supply to these leaflets. Three pockets with graded injury were established, and muscle morphology and vascular remodeling were monitored in 3 experimental groups: muscle leaflets without any treatment (Group 1, n = 6) that served as controls; muscle leaflets integrated with a fibrin interlayer (Group 2, n = 6); and leaflets integrated with fibrin and entrapped pyrrolostatin (Group 3, n = 6). We applied the fibrinogen and thrombin solutions, which polymerize to form a three-dimensional meshwork joining the tissues, creating a provisional matrix for angiogenesis, and acting as a delivery depot for agents aimed at minimizing ischemia-reperfusion lesion formation. After 2 months, the muscle leaflets biointegrated with the fibrin interface showed none of the signs of necrosis or ischemia-reperfusion lesions seen in the controls. Although no angiogenic factors were incorporated, the fibrin interlayer rapidly (<2 weeks) became a densely vascularized tissue replete with a voluminous capillary network. In contrast, controls showed poor bonding between the tissues, muscle fiber deterioration, and a compromised vascular network. Muscle structure was best preserved and angiogenesis was greatest when pyrrolostatin, a free radical scavenger, was added to the fibrin meshwork to reduce damage caused by overproduction of free radicals. This newly designed model will be useful to study many current approaches in cardiovascular biology, from pharmaceuticals to gene therapy, which might prove advantageous in muscle-designed cardiac assistance. **Key Words:** Cardiac assistance—Skeletal muscle model—Muscle damage—Ischemia-reperfusion prevention—Fibrin interlayer.

Heart failure as a significant health problem worldwide needs expanded treatment options. To date, heart transplantation is the most powerful therapy available for patients with end-stage heart failure. However, this option is limited by a shortage of donors and by immunological complications (1,2). Mechanical cardiac assist devices have been developed as a bridge to transplantation or as a bridge to recovery. Although their availability and quality are progressively increasing, clinical trials consistently demonstrate a high frequency of device-related complications (3–5), largely due to tissue/blood incompatibility with the artificial biomaterials from which they are constructed. By using autologous skeletal muscle for cardiac contractile support, we can avoid these compatibility obstacles as well as provide a potentially valuable secondary blood source to the impaired heart.

More than a decade ago, dynamic cardiomyoplasty was introduced in clinical practice as a viable alternative treatment for the failing heart. In this procedure, a pedicled skeletal muscle flap, usually the latissimus dorsi muscle (LDM), is wrapped around the heart and paced in synchrony with the ventricular contractile cycle (6–8). A major and hotly disputed topic in enhancing cardiomyoplasty success is the importance of maintaining adequate LDM structure and function after its mobilization (6,7,9). Dissection of important blood supply routes, and resultant ischemia, underlie many of the complications of using muscle flaps in cardiomyoplasty. Considerable experimental evidence points toward endothelial dysfunction as a central event in ischemia-

Received February 1999; revised July 1999.
Address correspondence and reprint requests to Dr. Victor V. Nikolaychik, Clinical Professor of Medicine, University of Wisconsin Medical School, 112 E. Freistadt Road, Suite F, Theinsville, WI 53092, U.S.A.

reperfusion tissue injury (9,10). Clinical experience shows a poor natural angiogenic response after cardiomyoplasty, whereby the traumatized, ischemic LDM and the dynamic myocardial wall do not bond tightly to each other, and vascular connections between these 2 tissues are poorly established (9,10). We hypothesize that employing novel pharmacological approaches to enhance the natural angiogenic processes occurring at the juxtaposition of these disparate tissues can improve the functional status of these muscles, and thus more fully realize the desired benefits of cardiomyoplasty.

We have previously employed an in vivo sheep model as a means to evaluate changes in muscle structure and in tissue interactions at the LDM/heart interface after cardiomyoplasty (9,11). The goals of the present study were to develop an uncomplicated surgical research design for creating LDM flaps with graded and controlled ischemic injury; to test the efficiency of a new tissue-compatible interlayer, based on fibrin meshwork, for enhancing physical and vascular associations between 2 muscle sections; and to examine new pharmacological approaches to mitigate ischemic damage in the mobilized LDM.

MATERIALS AND METHODS

Surgical procedure

Animal preparation

The surgical procedures have been described in detail previously (11). Briefly, all animals underwent general anesthesia induced with bolus diazepam (5 mg/kg i.v.) and sodium thiopental (20–25 mg/kg i.v.). The animals were intubated, placed on a Drager ventilator (North American Drager, Telford, PA, U.S.A.), and maintained on halothane gas anesthesia (1.2% with 4 L/min O_2). The oxygen saturation level and heart beat rate were monitored via a pulse oximeter placed on the animal's tongue.

Preparation of LDM pockets

Eighteen St. Croix sheep weighing 27–43 kg were randomly divided into 3 groups of 6 animals in each: Group 1 had apposed muscle leaflets without any treatment that served as controls; Group 2 had muscle leaflets integrated with a fibrin meshwork interface, and Group 3 had LDM leaflets integrated with fibrin containing pyrrolostatin, a free radical scavenger, entrapped within the fibrin meshwork.

The animals were placed in a lateral position, and a longitudinal skin incision was made from the right axilla toward the costovertebral angle. At first, a 6 × 16 cm flap of subcutaneous adipose tissue was dissected from the medial, lateral, and proximal sides, leaving the distal aspect connected to adipose tissue around the external oblique muscle and iliac crest. This severs the primary vessels supplying the adipose flap, rendering the tissue largely avascular. This is important for our model because this adipose flap served as a dividing lamina between the mobilized LDM leaflets, and a patent preexisting adipose vasculature might provide collateral ingrowth into the juxtaposed muscle tissue, thereby complicating our assessment of vascular regeneration within the muscle tissues.

The second step was ligation of the vessels originating from the intercostal arteries that penetrate the lateral segment of the LDM, followed by mobilization of this section (leaflet M), similar to the standard technique of subtotal mobilization of LDM (6–8). Vessels entering the LDM from the spinal posterior, the profound posterior, and the superficial anterior areas were not disturbed; therefore, the stationary leaflet S, comprised of the transverse and oblique segments of the LDM, had an undisturbed vascular supply (Fig. 1A and B).

The dividing adipose tissue lamina was then placed on top of the in situ oblique LDM segments, and the ischemic, mobilized leaflet M was positioned on top of this dividing lamina. All 3 tissue layers

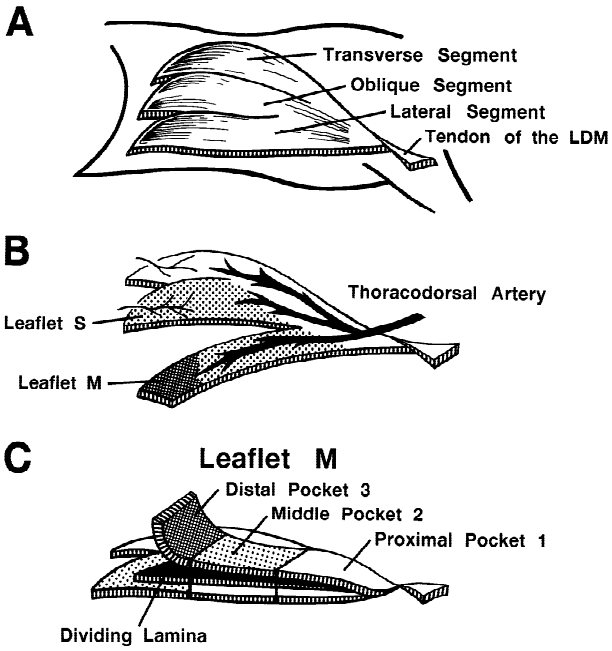

FIG. 1. The schematic drawing shows the experimental design: Overall view of the right latissimus dorsi muscle **(A)**; formation of 2 leaflets and territories vascularized by thoracodorsalis artery thereafter (darker area corresponds to severe ischemia) **(B)**; and experimentally generated pockets **(C)**. The outline indicates the border where pockets have been formed between the dividing adipose tissue.

were sutured together, forming 3 *sandwich* pockets in the proximal (Pocket 1), middle (Pocket 2), and distal (Pocket 3) regions in the juxtaposed LDM leaflets (Fig. 1C). Finally, the distal part of the ischemic leaflet M was sutured to the lumbarodorsal fascia to provide physical immobilization.

Autologous fibrin-meshwork interface

In the past, fibrin meshwork has been used as a *passive* tissue glue in many surgical procedures that required prevention of postsurgical leaks, filling of void spaces, or good attachment of tissues (12). Fibrin glue has also previously been used in cardiomyoplasty procedures to prevent seroma formation after transposing the LDM (13). More recently, we tested a fibrin-based interface between mobilized LDM and myocardium as a supportive element in dynamic cardiomyoplasty (10).

The fibrin meshwork was formed by thrombin treatment of its protein precursor, fibrinogen, which was prepared from fresh-frozen citrated autologous blood using standard plasma cryoprecipitation procedures (12). Forty-five ml of frozen plasma was thawed over 6 h and centrifuged at 2,500 rpm (Beckman J6M) to produce between 1.2 and 1.6 ml of viscous cryoprecipitate. Protein constituents of cryoprecipitate include primarily fibrinogen, fibronectin, vitronectin, factor XIII, and albumin (12). A solution with a final fibrinogen concentration of 15 mg/ml was created by dilution with sterile water. Lyophilized bovine thrombin (GenTrac Inc., Middletown, WI, U.S.A.) was in buffered saline solution to a final activity of 100 U/ml. Two different syringes were filled with either the thrombin or the autologous fibrinogen solution and were combined in equal volumes via a Y-connector at the time of application into the space between the muscle leaflets and the dividing lamina (Group 2). In Group 3 animals, pyrrolostatin (final concentration 10 mM) was added to the fibrinogen solution before fibrin-meshwork formation. The total volume of the fibrinogen–thrombin mixture introduced in each pocket was 2.0 ml. Animals in which muscle leaflets and adipose laminae were apposed without a fibrin-meshwork interlayer served as controls.

Transmission electron microcopy and morphological assessment

Conventional electron microscopic techniques were used to assess morphological details within the muscle, focusing on evidence of angiogenesis and ischemic damage in different fields of the LDM. Briefly, biopsy specimens (3 × 4 mm) were excised at various time points following surgery, placed into Karnovsky's fixative, postfixed in 1% osmium tetroxide, dehydrated through a graded series of ethanol and acetone, and embedded in Spurr resin. Ultrathin sections (60–90 nm), stained with 5% uranyl acetate and Reynold's lead stain, were examined with a Philips 400T transmission electron microscope using an accelerating voltage of 60 kV. Eight electron micrographs of 2 randomly selected areas within each pocket were evaluated, focusing on the extent of gross ischemic tissue damage, ultrastructural morphology of the muscle, dividing adipose lamina, interposed vasculature, and the fibrin interlayer when present, as well as on the overall capillary density within these tissues. Routine staining of semithin sections with toluidine blue was also carried out in the areas of interest to count capillary numbers. In selected experiments, capillary numbers were assessed after conventional indirect immunoperoxidase staining of endothelial cells for von Willebrand factor (11).

RESULTS

Gross anatomical characteristics of control LDM leaflets

Prior to formulating the new surgical model, we measured the basic linear parameters of whole LDM leaflets immediately after mobilization. The length of the free LDM leaflet M was 16 ± 3 cm, and its width was 5 ± 2 cm. The large size of both the S and M leaflets allowed us to easily generate 3 distinct large area pockets separated by suture lines. The mean lengths of the proximal, middle, and distal pockets (Pockets 1, 2, and 3) were approximately 7, 5, and 4 cm in length, respectively (Fig. 1). The basis for such nonuniform tailoring stemmed from the unique surgical procedure and anatomical features present. The LDM has 2 important blood supplies: the thoracodorsal artery is the major source, and the intercostal and lumbar arteries function as secondary supplies. In the mobilized leaflet M, vascularization is reduced to dependency upon the thoracodorsal artery as the sole supplier of blood. This situation mimics the vascular conditions within the lateral section of the LDM when it is mobilized for cardiomyoplasty while the other static leaflet S remained in situ with a patent vascular supply and served as a control (Fig. 1B).

To identify vascular changes due to surgery, we used a nondestructive staining technique whereby regions of LDM vascularized by the thoracodorsalis artery were visualized by Evans Blue dye, injected into this artery both before and after mobilization of

LDM. As depicted in Fig. 1, the thoracodorsalis artery vascularized approximately 75% of the nonmobilized LDM whereas in the mobilized LDM this artery only perfused about 60% of the muscle volume, as determined by tissue permeation with the injected dye. This reduced vascular supply is a result of surgical trauma and subsequent vessel contraction. After ligation of the perforating vessels of LDM leaflet M, the distal region of this leaflet was rendered highly ischemic and demonstrated marked cyanosis, as inferred by negligible staining with Evans Blue dye. The middle region of leaflet M appeared slightly cyanotic and was diffusely stained. The border between nonstained and diffusely stained areas determined the suture position to demarcate pockets 2 and 3 (Fig. 1C). Stationary leaflet S manifested moderate cyanosis at the traumatized edges in the vicinity of Pockets 2 and 3, which disappeared after 3 h. Proximal regions of both leaflets were intensely stained with Evans Blue, and delineated the suture line for creating proximal Pocket 1. While in stationary leaflet S, a patent blood supply was maintained to all regions of the muscle; this procedure generated in mobilized leaflet M a graded deprivation of vascular supply (increasing from proximal to distal aspects), resulting in variable induction of ischemia.

In developing novel cardiomyoplasty procedures employing transposed LDM, it was initially presumed that after the initial postoperative trauma, natural revascularization of the LDM would allow maintenance of normal muscle bundle structure and contractile function so that it could efficiently enhance cardiac output from the weakened heart. In our control series, however, we noted the significant time-dependent decrease in the size of the ischemic leaflet M following mobilization. Because the length and width of leaflet M were fixed at controlled dimensions by suturing of the distal end, only the LDM leaflet thickness was changed. At 14 days postsurgery, although measured muscle leaflet M thicknesses tended to be slightly reduced from values obtained during surgery, these differences were not statistically significant (Table 1). After 56 days, however, although the thickness of the proximal and middle regions of leaflet M were not further reduced, marked muscle degeneration continued in the highly ischemic distal leaflet 3M, whose thickness was dramatically decreased to 2 ± 1 mm, approximately 25% of its starting thickness.

Throughout the 56 day experimental series, there was no strong bonding observed between the dividing adipose lamina and pockets 2M and 3M. In the less-ischemic pocket 1M, however, tissue apposition appeared well established at experimental termination. In contrast, the nonischemic leaflet S developed firm connections with the separative adipose lamina in all regions of association. These observations prompted further investigation, at the ultrastructural level, of the pathological processes that mediated the altered morphology of the mobilized skeletal muscle and its reduced structural integration with apposing tissues.

Ultrastructural observations in the control LDM leaflets

To further elucidate LDM tissue responses to graded ischemia, we examined, via electron microscopy, ultrastructural characteristics present in both intact LDM and in leaflets S and M from Group 1 animals (Fig. 2).

Numerous capillaries surrounded muscle fibers in the intact LDM (Fig. 2A). These endothelial cells contained typical cytoplasmic organelle constituencies and had prominent nucleoli. There were tightly apposed intercellular junctions between endothelial cells, and these cells were abluminally enveloped by a clearly visible and continuous basement membrane and were often encircled by pericytes. Muscle fibril organization appeared normal, and sparse collagen fibers were present in the interstitium. Overall, it appeared that, as expected, the comprising endothelial cells in the control LDM were morphologically typical of those seen in the vascular bed of mature skeletal muscle.

TABLE 1. *Thickness of LDM pockets in mobilized leaflet M (mm)*

Conditions	Proximal pocket	Medial pocket	Distal pocket
Control, after mobilization	13 ± 2	10 ± 2	7 ± 1
Control, 14 days postsurgery	9 ± 2	8 ± 3	6 ± 2
Control, 56 days postsurgery	10 ± 3	7 ± 1	2 ± 1[a]
Biodesign with fibrin meshwork	11 ± 3	8 ± 2	5 ± 1[b]
Fibrin meshwork with pyrrolostatin	11 ± 3	9 ± 2	7 ± 1[b]

[a] $p < 0.05$ vs. control pocket immediately after immobilization.
[b] $p < 0.05$ vs. control, 56 days postsurgery.

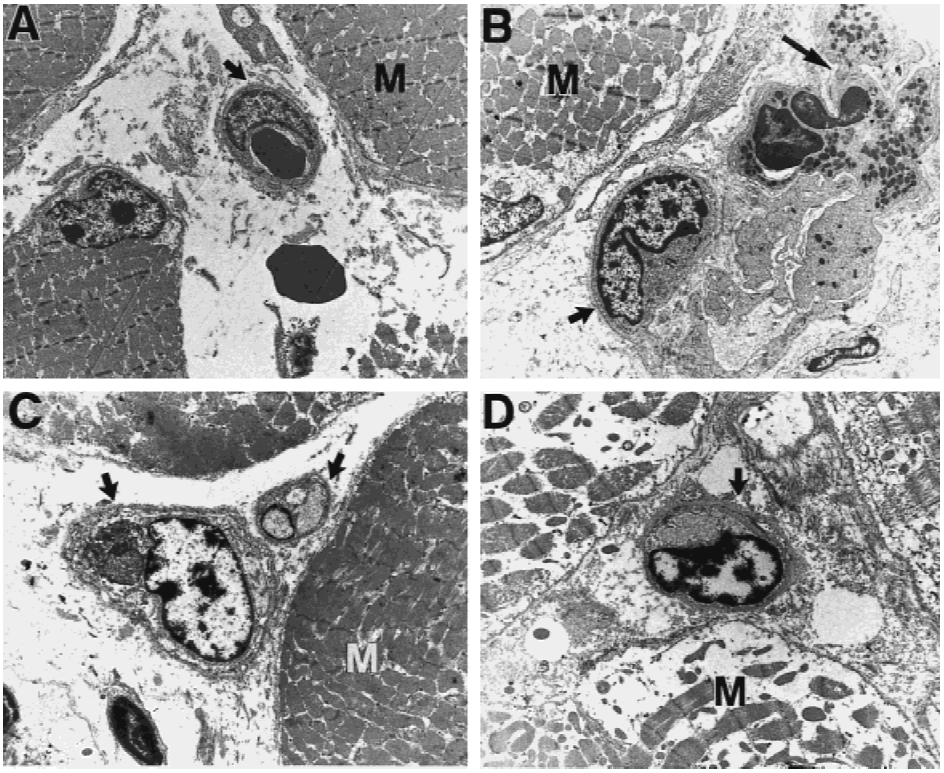

FIG. 2. Transmission electron microscopy of muscle tissue is shown. The time course of pathogenic events in poorly vascularized nontreated leaflet 3M is shown in a control specimen, intact muscle (M) before mobilization **(A)**. Capillary morphology **(small arrow)** shows thin endothelial cells with prominent intercellular clefts and cytoplasmic vesicles (×2,800). Shown is a specimen taken 3 h after mobilization **(B)**. The LDM myofiber structure is preserved; however, capillary structure is severely compromised by marginating neutrophils **(large arrow)**. Note the endothelial cytoplasmic folding and projections in the damaged capillary (×3,600). A specimen taken at Day 14 **(C)** shows destruction of muscle tissue and alterations in capillary appearance: processes on the luminal surface and basal membrane irregularity are present (×2,800). Devastating damage of muscle and capillaries at Day 56 is shown. Interstitium contains copiously deposited collagen bundles (×3,600) **(D)**.

In contrast to the intact LDM, ultrastructural examination of biopsy specimens from surgically treated leaflet M showed degenerative changes that progressed with both the extent and time of ischemia as reflected in gross degeneration of muscle bundle structure and of the microvascular network that supplied it (Fig. 2B–D). Even at very early time points (3 h postsurgery), when biopsy specimens were excised from these leaflets, the amount of resultant bleeding appeared proportional to the amount of Evans blue staining, and thus vascularization, present in the various regions. For example, specimen excision from pockets 2M and 3M resulted in only slight blood loss whereas biopsy of lM and all of the leaflet S pockets resulted in copious bleeding. With time, muscle regions with the most compromised blood supply showed the most marked degenerative alterations in both their muscle fiber architecture and in their vasculature. Immediately following the mobilization procedure, localized muscle deterioration and vascular damage due to surgical trauma were observed at the incisional margins of pockets 2M and 3M. Within 3 h postsurgery, leukocyte margination and extravasation became obvious in the most ischemic regions of leaflet M, associated with compromised microvascular patency (Fig. 2B). By Day 14, we observed disorganization of the myofibrillar cytoarchitecture in distal pocket 3M, with some areas showing frank loss of fiber striation (Fig. 2C). This was not a fixation artifact as earlier light microscopic evaluation supported the current EM observations. The Z lines and A bands were still observed in these patchy areas, but their structural disintegration progressed with time such that, beyond Day 28, this tissue was rendered essentially noncontractile (Fig. 2D). In strong contrast, throughout the 56 day duration of this experimental series, no gross degenerative changes were observed in electron micrographs of specimens from the proximal pockets of the mobilized leaflet M or in any regions of the stationary leaflets.

It has long been recognized that the major initial morphological alterations following ischemia-reperfusion develop in the microvasculature (14–17). Figure 2 illustrates the typical temporal relationships of this vascular compromise that coexist along with the muscle degeneration in ischemic pocket 3M. Within hours after mobilization, the endothelial cells within the LDM vasculature began thickening, becoming rounded or cuboidal in shape, and their plasma membranes appeared disrupted with discontinuous intercellular margins. In severely damaged cells, cytoplasmic vacuolar accumulation, and mitochondrial swelling and destruction of cristae were other characteristics frequently observed in conjunction with gross tissue edema (Fig. 2B and C). Inter-

estingly, apparently normal endothelial cells were often observed directly adjacent to the swollen, damaged endothelial cells, suggesting variable responses amongst these cells to ischemic conditions. All of these early vascular changes were associated with an increased frequency of neutrophil margination and diapedesis out of the affected vessels, supporting their purported critical role in mediating the early sequelae of ischemia-reperfusion (14).

By 14 days postprocedurally, biopsies taken from pocket 3M demonstrated considerable destruction of a large fraction of both its muscle tissues as well as its associated microcirculation. Endothelial intercellular junctions were disrupted, and the vast majority of the capillary bed appeared necrotic (Fig. 2C). At 28 days and beyond, essentially all of the few remaining endothelial cells exhibited morphological degeneration of their intracellular components and alterations of their plasma membranes, characterized by a large frequency of cytoplasmic projections extending into the capillary lumen (Fig. 2D). A quantitative representation of this microvascular degeneration is depicted in Table 2 whereby the total capillary cross-sectional area in the medial and distal regions of the mobilized LDM leaflet was markedly reduced, 56 days postsurgery, to approximately 40% of starting values. Although the distal section of the stationary leaflet also displayed some capillary loss over this time frame, the reduction in vascularization here was not nearly as pronounced as in the surgically transposed muscle. Muscle bundle degeneration observed throughout this time course paralleled the decline of vascular patency in the affected regions.

After identifying the prominent pathological events (Table 3) in LDM degeneration due to mobilization, vascular insufficiency, and muscle disuse, we began testing the efficacy of a bioengineered artificial matrix in structurally and functionally adjoining all of the layers of our LDM leaflet model.

Fibrin meshwork inhibits muscle degeneration in mobilized LDM

The angiogenic potential of healthy muscle is extremely high (15–17); however, as it was demonstrated earlier, different zones of the LDM have unequal residual ability to regenerate a sufficient vascular supply following mobilization. In an attempt to enhance innate angiogenesis and thus revitalize the LDM with a regenerated vascular network, we engineered a provisional matrix by introducing fibrin meshwork between the dividing lamina and the ischemic and nonischemic LDM leaflets (experimental Group 2).

In contrast to the marked temporal reduction in LDM leaflet thickness observed with time in animals not receiving this treatment, animals in which fibrin meshwork was introduced between the surgically divided tissue layers showed no overall decrease in muscle pocket dimensions observed at the 56 day endpoint of these experiments compared to nontreated controls. After application and polymerization of the fibrinogen–thrombin composition, we immediately observed firm and flexible physical connections between all 3 layers in all regions. This was maintained through Day 56 where good intertissue adhesion was achieved between both leaflets M and S and their adipose tissue dividing lamina even at the interface with the highly ischemic leaflet 3M. These findings revealed that the fibrin meshwork had rapidly developed strong bonding to both the muscle and adipose tissue and provided a durable and flexible interlayer for adjoining these tissues.

From electron micrographs of biopsy specimens taken from these Group 2 animals, it became obvious that the fibrin meshwork interstitium provided not only structural support but also served as an active component in restoring and maintaining functional vascular connections between the separate tis-

TABLE 2. *Capillary density in muscle of different leaflet regions (capillaries/mm^2)*

Conditions	Proximal pocket	Medial pocket	Distal pocket
Leaflet S control before immobilization	411 ± 56	507 ± 61	628 ± 42
Leaflet S, Day 56 postsurgery	478 ± 65	434 ± 33	402 ± 47[c]
Leaflet M control, before immobilization	389 ± 45	491 ± 28	554 ± 63
Leaflet M, Day 56 postsurgery	425 ± 51	234 ± 82[a]	208 ± 76[d]
Leaflet M, biodesigned with fibrin meshwork	455 ± 51	385 ± 66	412 ± 43[e]
Leaflet M, fibrin, pyrrolostatin	417 ± 39	431 ± 65[b]	478 ± 72[f]

[a] $p < 0.01$ control vs. 56 days postsurgery.
[b] $p < 0.05$ 56 days postsurgery vs. fibrin/pyrrolostatin.
[c] $p < 0.01$ control vs. control.
[d] $p < 0.01$ control vs. 56 days postsurgery.
[e] $p < 0.05$ 56 days postsurgery vs. biodesigned leaflet.
[f] $p < 0.01$ 56 days postsurgery vs. fibrin/pyrrolostatin.

TABLE 3. *Different pathological conditions in the modeled pockets*

	Pocket 1	Pocket 2	Pocket 3
Leaflet M	Noncompromised vasculature	Moderately compromised vasculature	Critically reduced blood supply, practically avascular
	Light transitory ischemia	Local ischemia-reperfusion damage	Global and persistent ischemia
	Normal muscle tissue structure	Local necrosis of muscle tissue	Frank atrophy of muscle fibers and gross fibrosis
Leaflet S	Noncompromized vasculature	Minimally compromised vasculature	Minimally compromised vasculature
	Light transitory ischemia	Moderate short-term ischemia	Moderate short-term ischemia
	Normal muscle tissue structure	Normal muscle tissue structure	Normal muscle tissue structure

sue layers (Fig. 3B and D). In the highly ischemic region of leaflet M, although occasional areas of muscle deterioration were recognized at and beyond 14 days, the extent and severity of such damage was significantly reduced compared to similar sections in Group 1 animals that did not receive the fibrin interface therapy. The beneficial effects of the incorporated fibrin meshwork on overall muscle tissue vitality were maintained through Day 56 (Fig. 3A) and mitigated the gross thinning of the mobilized muscle leaflet that occurred with time (Table 1). Ultrastructural examination of the fibrin meshwork interface revealed that it had effectively allowed ingrowth and incorporation of various cellular constituents, in effect resulting in the development of a lasting viable and biologically active neotissue layer as opposed to merely an inert proteinaceous physical connecting layer. With time, an increasingly complex vascular network formed within the fibrin scaffolding, consisting of blood vessels of various diameters, some of which were visible to the naked eye during biopsy excision. During Days 14 and 56 biopsies, considerably more bleeding was noted from excision sites in the most distal Pocket 3 of both leaflets S and M in the fibrin-treated versus control animals, supporting a role for the fibrin interface in promoting vascularization of the traumatized LDM. This was obviated at the microscopic level whereby poor natural revascularization occurred at the interface region of distal pocket 3M of control animals (Fig. 2C) whereas an extensive vascular network developed throughout the fibrin interlayer of the fibrin-treated animals (Fig. 3A and B). Quantitatively, the protective effect of fibrin was reflected in a two-fold increase in capillary density in the most ischemic regions of leaflet M after 56 days compared to control animals (Table 2).

Neovascularization of the fibrin matrix likely necessitates the involvement of various other cells in addition to endothelial cells. In addition to endothelial cells, a variety of other cell types, including fibroblasts, smooth muscle cells, pericytes, and occasional mast cells and leukocytes also migrate into the interlayer, and likely play important roles in the development of this matrix into a functional tissue (Fig. 3D). Although endothelial cell migration and organization into capillaries are fundamental characteristics of angiogenesis, cytokines, growth factors, and extracellular matrix components produced by these other cell types are probably critical in initiating and orchestrating these angiogenic events. Endothelial cells within the fibrin matrix appeared normal in morphology and ultrastructure and were in close apposition to their neighboring cells. Occasionally observed thick cytoplasmic protrusions into the vessel lumen may be indicative of ongoing intussusceptive capillary development. In several sections, longitudinal views of capillaries consisting of 3 or 4 tightly adjoined endothelial cells were visible that often contained erythrocytes within their lumens, implying their ability to transport oxygen and nutrients to the surrounding tissues. Basement membranes with distinct boundaries were present around all of the capillaries. The endothelial cells actively formed endocytotic vesicles (Fig. 3C), indicating the existence of active transport mechanisms operating across the plasma membrane. Pericytes enveloped many of the capillaries and were closely apposed to the endothelial cell basement membrane. Considering the accepted role of pericytes in regulating blood flow from arterioles into capillary beds (15–17), we propose that these association sites are markers for the advanced level of development of a functional microvascular network, replete with intact flow regulatory mechanisms. The marked similarity to vascular smooth muscle cells has led to the theory that pericytes as pluripotent cells may be precursors of muscle cells because capillaries are remodeled into larger vessels that contain large numbers of smooth muscle cells (17). Indeed, by Day 56, we often observed the infiltration into the fibrin matrix of blood vessels of significanly larger diameter than typical skeletal muscle capillaries. Whether these represent structures precursory to macrovessels of more complicated design or if they are simply large bore capillaries remains to be determined.

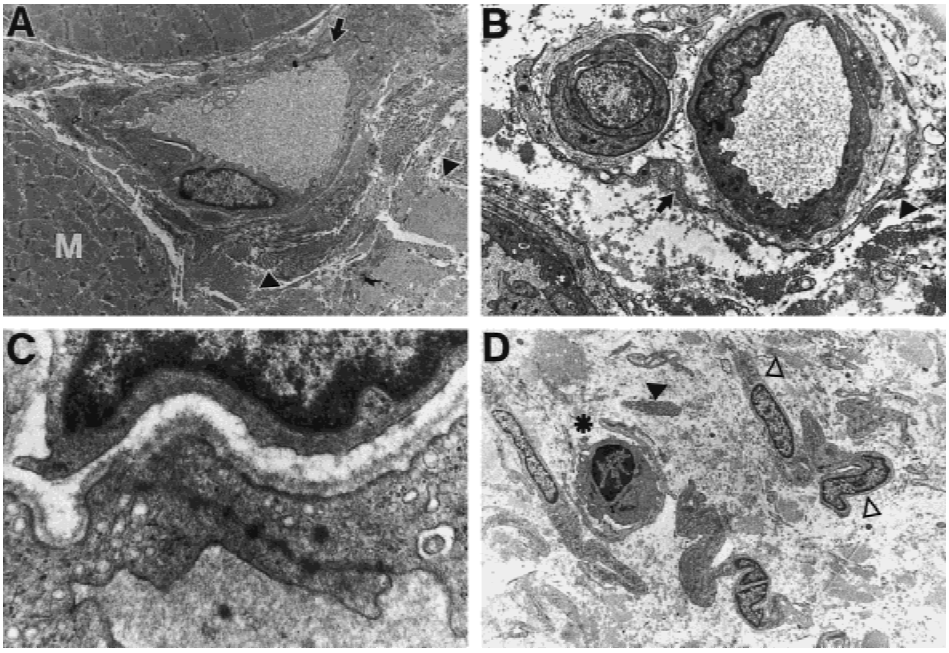

FIG. 3. Transmission electron microscopy shows distan leaflet 3M and fibrin interface. The muscle structure of bioengineered leaflet 3M at Day 56 is depicted **(A)**. Fibrin meshwork penetrated between muscle bundles. Large bore capillaries with normal structure exist in muscle; there is no indication of endothelial cell swelling or detachment from their basement membrane. Numerous collagen fibers in transverse and longitudinal projections are present **(arrow head)**. A representative area of fibrin interlayer at Day 56 is shown **(B)**. Mature and sprouted capillaries are presented. Pericapillary space is enriched with collagen fibers. Adjacent endothelial cells are in tight contact with each other (×2,800). The capillary wall contains vesicles, some of which are open to the cytoplasm; the others are open to the basement membrane **(C)**. In this particular section, the vesicles are more numerous toward the basement membrane than toward the lumen (×36,000). The structural composition of biodesigned interface is presented **(D)**. Shown are macrophages **(asterisk)** with ovoid nucleus and electron dense chromatin adjacent to the inner margin of the nuclear membrane; dense cytoplasmic granules and numerous cytoplasmic extensions reflect moderate activation. This cell is seen in close proximity with a fibroblast **(arrow head)**. Typical fibroblasts with deep nuclear indentations and collagen rich extracellular matrix are found within the interlayer and dividing lamina areas (×2,800).

Fibroblasts were frequently observed in the fibrin matrix, both in the interstitial regions and in the immediate vicinity of the developing vasculature. These cells could have multiple functions in the maturation of this newly forming tissue. Secreted cytokines and growth factors could act in a paracrine fashion to modulate the proliferation, migration, and differentiation of endothelial cells during angiogenesis. In addition, fibroblasts produce and deposit into the interstitium large quantities of extracellular matrix proteins that can modulate both the structural properties of the interlayer as well as the biological activities of other resident cells (17). Fibers of typical collagen and elastin morphology, likely of fibroblast origin, were abundantly present in the maturing interlayer (Fig. 3), and are certainly critical determinants of the stress/strain characteristics of the remodeled fibrin scaffold.

Free radical scavengers enhance LDM revascularization

Reperfusion of ischemic tissues results in a generative burst of oxygen-derived free radicals, which is significanly correlated to impaired functional recovery of the affected tissues (14). Free metal ions serve as ideal templates for electron transfer reactions involving free radicals. In particular, free iron facilitates the production of the extremely toxic hydroxyl radical from the less harmful superoxide radical. In traumatized or diseased muscle tissue, the primary sources of free iron are hemoglobin and myoglobin from damaged erythrocytes and myocytes, respectively. We hypothesized that our fibrin interlayer could present a physical barrier to the extravasation and subsequent lysis of erythrocytes, thus reducing tissue damage that is catalyzed by iron-mediated free radical generation. However, fibrin meshwork alone was not sufficient to completely protect tissue from ischemia-reperfusion damage, and additional means were instituted. Fibrin meshwork has an excellent potential for serving as a delivery vehicle for various pharmacological agents (18). In an attempt to inhibit the noxious effects of free radical accumulation, we added pyrrolostatin, a free radical scavenger and inhibitor of lipid peroxidation (19), to the fibrin formulation used in Group 3 animals. This preparation resulted in similar fibrin meshwork polymerization and strong physical bonding characteristics between leaflets, as was observed in Group 2 animals. Importantly, inclusion of this agent resulted in additional preservation of the morphological structure of muscle tissues in distal pocket 3M (Fig. 4), compared to Group 2 animals receiving fibrin-only bioengi-

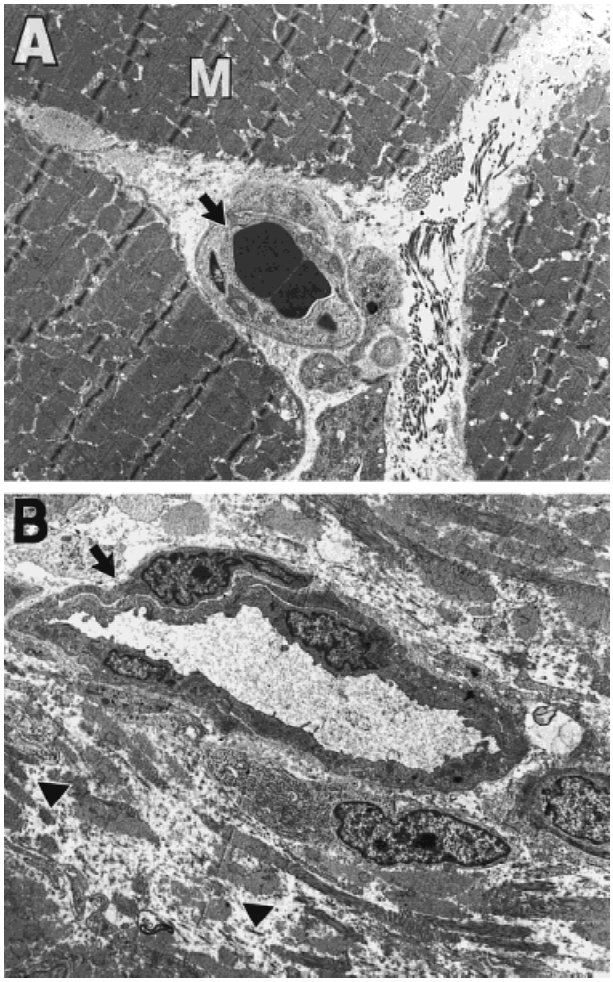

FIG. 4. Transmission electron micrographs demonstrate the protective effects of pyrrolostatin in leaflet 3M. A representative area of muscle is shown **(A)**. Well-preserved muscle tissue contains a mature capillary surrounded by mature basement membrane and pericytes. Muscle fiber damage, as reflected in the number of regenerative fibers, is minimal in this group (×4,600). An elongated, thin-walled, mature capillary penetrating within the fibrin interlayer is shown **(B)**. In contrast to immature capillaries containing exclusively endothelial cells, its morphology is more complex. This cross-sectional view shows 3 comprising endothelial cells with intercellular junctional areas exhibiting extensive membrane overlap. Cells resembling myofibroblasts or synthetic phenotype smooth muscle cells are closely apposed to the endothelium. Pericytes display characteristic prominent nuclei surrounded by thin cytoplasm; these cells exhibit membranous interdigitations with endothelial cells (×2,800).

neered protection (Fig. 3). The combination of fibrin meshwork and pyrrolostatin also resulted in significantly enhanced vascularization in the LDM leaflets and in the fibrin interlayer, as inferred from measurements of capillary cross-section area in biopsy samples (Table 2). After 56 days, large bore vessels as well as an extensive capillary network were prominent features within the fibrin interlayer and the dividing lamina. This angiogenic response was significantly different from both the control group, where only sparse vascular regeneration was noted even after 2 months, as well from the animals that received fibrin matrix only, thus demonstrating the potential therapeutic benefits of inhibiting free radical accumulation in these healing tissues.

DISCUSSION

Skeletal muscle flaps are already being implemented in clinical efforts to enhance cardiac output via cardiomyoplasty and aortomyoplasty procedures (6). To date, however, these attempts to improve cardiac function by assisting the contractile mechanics of a weakened heart with superimposed, adjoined, and electrically paced skeletal muscle flaps have demonstrated several important shortcomings (10). Critical barriers to achieving the optimally expected benefit of such procedures include skeletal muscle degeneration secondary to ischemia caused by surgical mobilization and vascular isolation, poor establishment of biological (i.e., vascular) connections between skeletal muscle and the underlying heart tissue, and mechanical incongruities between the transposed skeletal muscle and the complex contours of the heart surface. In this article, we detailed the development of a novel in vivo model in which we can observe and clarify the biological mechanisms that are responsible for suboptimal performance of standard cardiomyoplasty procedures as well as test various interventional strategies designed to alleviate these detrimental pathological sequelae (10).

Sheep are a good animal selection for modeling human cardiomyoplasty operation, as their LDM experiences pathological changes following mobilization that are similar in quality and time course as in humans. In addition, the contractile properties of their LDM are more similar to those of humans than are other animal models. For example, we previously compared the fatigue resistance of sheep and dog LDM, as examples of nonathletic and athletic muscles; during a 30 min fatigue test, sheep LDM lost 43 ± 8% of its initial contractile force, close to what might be expected in humans, in comparison to only a 18 ± 5% loss in the dog muscle (20). Finally, the sheep's sedentary temperament and physical activity approximates that of a person recovering from surgery.

The anatomical arrangement of LDM facilitated our design of a simplified muscle leaflet model. This muscle consists of 3 segments: the transverse, oblique, and lateral as shown in Fig. 1. The transverse segment is situated very deep, close to inferior

scapular angle, and arises from the aponeurosis of the spinal processes of T-6 through T-9, often fusing with the teres major and posterior serratus inferior, thus making dissection difficult. The oblique segment arises from the thoracodorsalis aponeurosis of T-9 through T-12, and shares several common branches of the intercostal arteries with the external oblique muscle, similarly complicating its mobilization. The lateral segment arises from the lower 2 ribs and lumbodorsal fascia and is 5–7 cm in width and 25–30 cm in length in sheep. In contrast to the transverse and oblique sections, the lateral LDM is very accessible, easily dissected free, and its mobilization does not jeopardize vascularization of surrounding tissues. The lateral LDM is consistently supplied by 1 primary branch of the thoracodorsalis artery whereas variably numbered multiple branches supply the oblique section of the LDM (21).

With mobilization, however, vessels that supply 60 to 70% of the blood flow to the middle and distal regions of the lateral LDM are severed, rendering these areas underperfused and ischemic (22). This decrease in regional blood flow results in significant depression of contraction velocity and power generation in affected regions, obviated by the muscles declining resistance to fatigue (22,23). These data are consistent with our ultrastructural observations describing graded ischemic damage in the mobilized tissue (Table 3). Degeneration of any region of the transposed muscle will have a detrimental effect on the capacity of the whole muscle flap to perform the work that is required for providing effective cardiac assistance. Indeed, in the absence of special efforts to enhance revascularization, the most ischemic tissues (distal region of leaflet M) suffered extensive damage that progressively worsened.

By incorporating a layer of rapidly polymerizing fibrin sealant between 2 tissue layers, we not only provided an immediate measure of physical bonding between disparate tissues but also created a three-dimensional scaffolding into which various cellular constituents migrated and set up residence, ultimately resulting in the generation of a complex and functional neotissue. This living interlayer developed abundant vascular connections with the damaged skeletal muscle, and reversed the progressive necrosis that was initiated by surgically induced ischemia. The inclusion of pyrrolostatin in the fibrin matrix to bind free iron reduced the generation of free radicals in the wound locale, and resulted in additionally enhanced revascularization and concomitant preservation of muscle ultrastructural integrity. Thus, the beneficial effects of using a fibrin matrix in these procedures is enhanced by its ability to act as a delivery depot for various bioactive agents (10,18,24, 25). We propose that by incorporating a cocktail of proangiogenic factors and/or autologous endothelial cells into the fibrin matrix at the time of polymerization, we can further accelerate neovascularization of the fibrin interlayer and revascularization and recovery of the damaged skeletal muscle.

Another potential barrier to achieving the optimal benefits available with cardiomyoplasty is a mismatch in the mechanical properties of the 2 juxtaposed muscle tissues. In standard procedures, except at suture sites, there is no physical bonding of the mobilized LDM to the complex and varying contours of the heart surface. By incorporating a fibrin matrix between the skeletal muscle and adipose tissue flaps, we generated a crosslinked protein interlayer that bonded tightly to and connected both of these tissue types. With time, this layer was reorganized and colonized by a variety of cell types, events that were clearly discernable by electron microscopy. A prominent feature of the maturing matrix was the infiltration of fibroblasts and the subsequent replacement of the nebulous fibrin matrix with a highly organized collagen-rich de novo connective tissue, resembling in many ways typical wound granulation tissue. The fibrinogen concentration that we employed in this study was significantly lower than that used by others for investigating fibrin meshwork utility as a tissue adhesive (26–28). At these concentrations, the polymerized product exhibits sufficient strength and deformability to maintain a pliant physical connection between the LDM and the beating heart. Using higher fibrinogen concentrations might result in a sacrifice of the interlayer flexibility and result in constrictive interference of the heart contraction cycle. Thus, in selecting a fibrin formulation for enhancing cardiomyoplasty, one needs to recognize the importance of the tradeoff between meshwork tensile strength and elasticity. In addition to our ability to manipulate the interlayer composition, this surgical model allows us to test the effect of varying the initial positioning and resting tension of the LDM flap on LDM/heart muscle physical integration. These parameters are under the stringent control of the surgeon and can be modulated as seen fit.

In conclusion, our model provides both a means to further our understanding of the degenerative changes that are associated with LDM mobilization as well as a starting point for the rational design of new surgical and pharmacological approaches to improve the physical and functional integration between 2 disparate tissues. We anticipate that this model will prove to be extremely useful in realizing

the final goal of dynamic cardiomyoplasty, that is, optimizing the transfer of skeletal muscle-derived power to the heart as a means of improving cardiac output.

Acknowledgments: We appreciate the technical expertise of Dr. Gennady Tchekanov and Ms. Michelle Rieder. We also thank Ms. Judy Schattner for providing technical help and animal husbandry, and Mr. Brian Miller for his careful preparation of the figures in this article. This project was supported by The Milwaukee Heart Foundation.

REFERENCES

1. Magovern GJ, Magovern G, Maher T, Benckart D, Park S, Christlieb J, Magovern G. Operation for congestive heart failure: transplantation, coronary artery bypass, and cardiomyoplasty. *Ann Thorac Surg* 1993;56:418–25.
2. Rose EA. Current status of cardiac transplantation. In: Akutsu T, Koyanagi H, eds. *Heart replacement—artificial heart 5.* Tokyo: Springer-Verlag, 1996:387–9.
3. Westaby S. The need for artificial hearts. *Heart* 1996;76:200–6.
4. Watson JT. Implantable artificial heart systems. In: Akutsu T, Koyanagi H, eds. *Heart replacement—artificial heart 5.* Tokyo: Springer-Verlag, 1996:95–100.
5. Nosé Y, Ohtsubo S, Tayama E. Therapeutic and physiological artificial hearts: Future prospects. *Artif Organs* 1997;21:592–6.
6. Magovern GJ, Simpson KA. Clinical cardiomyoplasty: Review of the ten-year United States experience. *Ann Thorac Surg* 1996;61:413–9.
7. Moreira LFP, Stolf NAG, Braile DM, Jatene AD. Dynamic cardiomyoplasty in South America. *Ann Thorac Surg* 1996; 61:408–12.
8. Chekanov VS, Krakovsky AA, Buslenko NS, Riabinina LG, Andreev DB, Shatalov KV, Dubrovsky IA, Shetty K. Cardiomyoplasty: Review of early and late results. *Vascular Surgery* 1994;28:482–8.
9. Nikolaychik VV, Chekanov VS, Silverman MD, Samet MM, Schmidt DH. Successful dynamic cardiomyoplasty with pharmaceutical support. In: Akutsu T, Koyanagi H, eds. *Heart replacement—artificial heart 6.* Tokyo: Springer-Verlag, 1997: 498–502.
10. Chekanov VS, Nikolaychik VV. Suggestions for overcoming the weak points of cardiomyoplasty. *Ann Thorac Surg* 1996; 4:1245–7.
11. Chekanov VS, Tchekanov GV, Rieder MA, Eisenstein R, Wankowski DM, Schmidt DH, Nikolaychik VV, Lelkes PI. Biological glue increases capillary ingrowth after cardiomyoplasty in an ischemic cardiomyopathy model. *ASAIO J* 1996;42(Suppl):M480–7.
12. DePalma L, Criss VR, Luban NLC. The preparation of fibrinogen concentrate for use as fibrin glue by four different methods. *Transfusion* 1993;33:717–20.
13. Chachques J-C, Carpentier A. Postoperative management. In: Carpentier A, Chachques J-C, Grandjean PA, eds. *Cardiomyoplasty*. New York: Futura, 1991:131–8.
14. Maxwell SRJ, Lip GYH. Reperfusion injury: A review of the pathophysiology, clinical manifestations, and therapeutic options. *Int J Cardiology* 1997;58:95–117.
15. Hudlicka O, Brown M, Eggington S. Angiogenesis in skeletal and cardiac muscle. *Physiol Rev* 1992;72:369–417.
16. Tyml K, Mathieu-Costello O, Noble E. Microvascular response to ischemia, and endothelial ultrastructure, in disused skeletal muscle. *Microvascular Res* 1995;49:17–32.
17. Hansen-Smith FM, Hudlicka O, Egginton S. In vivo angiogenesis in adult rat skeletal muscle: Early changes in capillary network architecture and ultrastructure. *Cell Tissue Res* 1996; 286:123–36.
18. MacPhee MJ, Singh MP, Brady R, Akhyani N, Liau G, Lasa C, Hue C, Best A, Drohan W. Fibrin sealant: A versatile delivery vehicle for drugs and biologics. In: Sierra DH, Saltz R, eds. *Surgical adhesives and sealants. Current technology and applications*. Lancaster: Technomic, 1996:109–20.
19. Kato S. Pyrrolostatin, a novel lipid peroxidation inhibitor from Streptomyces chrestomyceticus. *J Antibiotics* 1993;46: 892–9.
20. Chekanov V, Tchekanov G, Rieder M, Silverstein E, Cheng Q, Smith L, Zander G, Jacobs G, McConchic S, Christensen C, Schmidt D. Force enhancement of skeletal muscle used for dynamic cardiomyoplasty and as a skeletal muscle ventricle. *ASAIO J* 1995;41:M499–507.
21. Krakovsky AA, Andreev DV, Chekanov VS. Anatomo–topographical study of latissimus dorsi muscle in the aspect of cardiomyoplasty operation. *J Grudn Serdechno–Sosudistoj Chirurgia (J Thorac Cardio–Vascul Surgery; Russia)* 1991;2: 20–2.
22. Cruz MP, Michele JJ, Mannion JD, Magno M, George DT, Santamore WP. Cardiomyoplasty. Latissimus dorsi muscle function and blood flow during isolation. *ASAIO J* 1997;43: 338–44.
23. Chekanov V, Tchekanov G, Rieder M, Nikolaychik V, Schmidt D. Improving cardiomyoplasty results: Muscle adaptation using an electrical stimulation protocol started immediately after mobilization. *Artif Organs* 1997;21:506.
24. Ferrara N, Davis-Smyth T. The biology of vascular endothelial growth factor. *Endocr Rev* 1997;18:4–25.
25. Svensson EC, Tripathy SK, Leiden JM. Muscle-based gene therapy: Realistic possibility for the future. *Mol Med Today* 1996;4:166–72.
26. Silver FM, Wang MC, Pins GD. Preparation and use fibrin glue in surgery. *Biomaterials* 1995;16(12):892–903.
27. Marx G. Kinetic and mechanical parameters of fibrin glue. In: Sierra DH, Saltz R, eds. *Surgical adhesives and sealants. Current technology and applications.* Lancaster: Technomic, 1996: 49–59.
28. Lontz JF, Verderamo JM, Camac J, Arikan I, Arikan D, Lemole GM. Assessment of restored tissue elasticity in prolonged in vivo animal tissue healing: Comparing fibrin sealant to suturing. In: Sierra DH, Saltz R, eds. *Surgical adhesives and sealants: Current technology and applications.* Lancaster: Technomic, 1996:79–90.